Structural investigation of $AgNbO_3$ phases using x-ray and neutron diffraction

2004 J. Phys.: Condens. Matter 16 2795

(http://iopscience.iop.org/0953-8984/16/16/004)

INSTITUTE OF PHYSICS PUBLISHING JOURNAL OF PHYSICS: CONDENSED MATTER

J. Phys.: Condens. Matter **16** (2004) 2795–2810 PII: S0953-8984(04)70069-7

Structural investigation of $AgNbO_3$ phases using x-ray and neutron diffraction

Ph Sciau[1], A Kania[2], B Dkhil[3], E Suard[4] and A Ratuszna[2]

[1] CEMES, UPR CNRS 8011, 29 rue Jeanne Marvig, BP 4347, 31055 Toulouse, France
[2] A Chelkowski Institute of Physics, University of Silesia, ulica Uniwersytecka 4, 40-007 Katowice, Poland
[3] Laboratoire Structures, Propriétés et Modélisation des Solides, CNRS-UMR8580, Ecole Centrale Paris, 92295 Châtenay Malabry Cedex, France
[4] Institute M von Laue–P Langevin, BP 156, 38042 Grenoble, France

Received 1 October 2003, in final form 23 February 2004
Published 8 April 2004
Online at stacks.iop.org/JPhysCM/16/2795
DOI: 10.1088/0953-8984/16/16/004

Abstract

The structures and phase transitions of $AgNbO_3$ were investigated using neutron powder diffraction and restricted single-crystal x-ray diffraction. Both methods have revealed the high temperature M_3–O_1, O_2–T and T–C phase transitions but have not given any significant evidence of low temperature M_1–M_2 and M_2–M_3 ones. The refinements of neutron diffraction patterns allowed us to determine the symmetry, space group and crystal structure for all phases except the O_1 one. The existence of structural disorder in the T and probably O_2 phases was found. The high temperature paraelectric phase transitions can be interpreted on the basis of consecutive condensation of oxygen octahedron tilts around the main axis. The ferroelectric and antiferroelectric behaviour has been associated with Ag and Nb cations. The reason why phase transitions between low temperature ferroelectric and antiferroelectric phases are not detectable by diffraction methods is discussed. The sequence of phase transitions in $AgNbO_3$ can then be understood in the framework of a long range and/or local order–disorder type arrangement.

(Some figures in this article are in colour only in the electronic version)

1. Introduction

Dielectric investigations of the $AgNb_{1-x}Ta_xO_3$ (ATN) solid solutions and composites on their base pointed to these systems as promising candidates for high frequency/microwave materials [1–4]. The experiments performed in the 1 GHz region indicated a dielectric permittivity of 430, a temperature coefficient of permittivity < 50 ppm K^{-1} and a Q-value of 700 for the $AgNb_{0.65}Ta_{0.35}O_3$–$AgNb_{0.35}Ta_{0.65}O_3$ composite [3]. In addition, dielectric investigations showed that in the ATN solid solutions, for non-ferroelectric phases, there

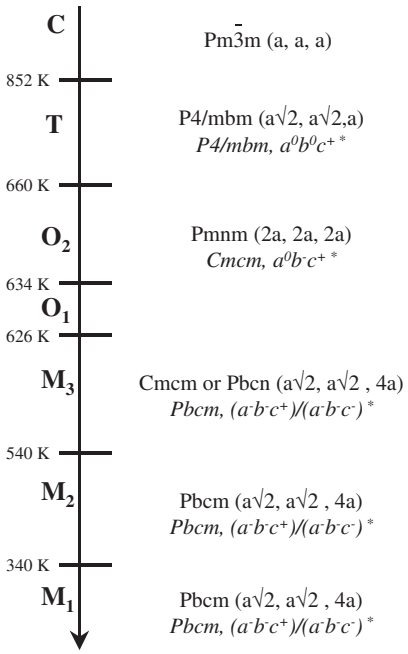

Figure 1. Sequence of the phase transitions of $AgNbO_3$ from [2, 10] and results of the present work (in italic*).

is a negligible dielectric dispersion for a very broad frequency range from 1 kHz up to approximately 100 GHz [1, 2, 5, 6]. These studies also showed that the suitable high dielectric permittivity originates from the contribution of the submillimetre relaxational mode to dielectric susceptibility [5, 7]. This relaxational mode appears in a very broad temperature range and is responsible for the appearance of a diffuse maximum of $\varepsilon(T)$ near the so-called M_2–M_3 phase transition [8]. The strength, frequency and temperature range of appearance of the relaxational mode strongly depend on Nb/Ta ratio. This phenomenon is most significantly seen in pure silver niobate $AgNbO_3$ [2, 5, 7].

A series of structural phase transitions is observed in $AgNbO_3$ [8–13]. This phase transition sequence is schematically drawn in figure 1. M_1, M_2 and M_3 denote the phases with orthorhombic symmetry in rhombic orientation while O_1 and O_2 are the phases with orthorhombic symmetry in parallel orientation. The parallel orientation means the orthorhombic axes are parallel to the pseudocubic directions, whereas in the case of rhombic orientation the orthorhombic *a*- and *b*-axes are parallel to diagonals contained inside the faces of the same pseudocubic axes [14]. T and C denote the phases with tetragonal and cubic symmetry, respectively. Figure 1 also contains the space groups and types of the pseudo-perovskite unit cell multiplication proposed in papers [2, 10]. These space groups were predicted on the grounds of group theory and the experimental x-ray and TEM results [10, 11]. It should be pointed out here that the space groups and the crystal structures of the particular phases have not been definitely determined yet. The temperature evolution of the lattice parameters and the sequence of phase transitions are similar to those observed in sodium niobate $NaNbO_3$ [14–18]. As in $NaNbO_3$, the phase transitions of $AgNbO_3$ were associated with two mechanisms of *displacive* phase transition: tilting of oxygen octahedra and displacements of particular

ions. The phase transitions between the high temperature paraelectric O_1, O_2, T and C phases are related to oxygen octahedron tiltings [10, 11]. The Nb ion displacements from the oxygen octahedron centre at the O_1–M_3 phase transition form the dipolar moments and the antiferroelectric state appears [9–11].

The high temperature M_3–O_1, O_2–T and T–C phase transitions were observed by x-ray [9, 10, 13], TEM [11], DTA and domain structure investigations [12]. The low temperature M_1–M_2 and M_2–M_3 phase transitions between ferroelectric M_1, antiferroelectric M_2 and M_3 phases were observed only as diffuse maxima of the $\varepsilon'(T)$ temperature dependence [6, 12]. In addition, in spite of the fact that the unquestionable appearance of ferroelectric and antiferroelectric states requires structural changes, the x-ray and TEM investigations have not revealed any detectable changes of symmetry between M_1, M_2 and M_3 phases [10, 11, 19]. Recently, the room temperature (M_1 phase) crystal structure of $AgNbO_3$ [20] was determined as isostructural with antiferroelectric $NaNbO_3$ [21]. However, it was pointed that this study could not distinguish between centrosymmetric $Pbcm$ and non-centrosymmetric $Pbc2_1$ space groups [20]. Nevertheless, an accurate x-ray diffraction study showed that the room temperature structures of $AgNbO_3$ and $NaNbO_3$ are very similar but not fully isomorphous [22]. These structural results showed that the crystal structures of the M_1, M_2 and M_3 phases are expected to be *antiferroelectric* or very close to *antiferroelectric* structure. Therefore, the transitions between these phases should be associated with slight modifications of this structure.

The appearance of the submillimetre relaxational mode in a very broad temperature range and the occurrence of two types of phase transition allowed us to postulate the coexistence of ordered and disordered subsystems in silver niobate [12, 23]. The former leads to normal sharp phase transitions; the latter leads to diffuse phase transitions. Therefore, the M_2 and M_3 phases were assumed to be disordered antiferroelectric [23]. The M_1 phase exhibits both weak ferroelectric and relaxor features [6, 23, 24]. Spectroscopic studies [4, 6] allowed us to postulate that disorder is related to the Nb ion sublattice. This means that the M_1, M_2 and M_3 phases may be characterized by different, static or dynamic, states of the Nb ion displacement subsystem. However, based on TEM studies [11] it was also proposed to connect the disorder evidenced above 500 K in $AgNbO_3$ with the O ion sublattice.

Due to the above statements, the knowledge of crystal structure of the particular phases, especially M_1, M_2 and M_3 ones, and the origin of the disorder in $AgNbO_3$ are very important questions for $AgNbO_3$-based materials such as ATN from both basic and application points of view. That is why the x-ray and neutron diffraction studies of pure $AgNbO_3$ are undertaken.

2. Experimental procedures

$AgNbO_3$ single crystals were grown by a flux method. The technological details have been described in paper [25].

X-ray studies were carried out at the *Structures, Propriétés et Modélisation des Solides* Laboratory (École Centrale Paris, France) with a high accuracy Microcontrol diffractometer using the graphite monochromatized Cu Kα radiation issuing from a 18 kW Rigaku rotating anode generator. Measurements were performed in reflection mode (θ–2θ scan and ω scan) on oriented single crystals. Two types of single-crystal plate were used: $(100)_c$ natural face (sample C1) and $(110)_c$ plates mechanically polished (sample C2). The samples were placed in a Rigaku furnace with a thermal stability better than 0.5 K.

Neutron experiments were performed on the D2B high resolution powder diffractometer at Institut Laue–Langevin in Grenoble. The monochromatic beam of $\lambda = 1.05$ Å was used. A powder sample was obtained by grinding single crystals. Approximately 2 cm^3 of powder

Table 1. Measurements and refinement conditions of neutron data.

Data collection	
Diffractometer	D2B (ILL)
Monochromator	Ge(115)
Instrument geometry	Debye–Scherrer
Temperature (K)	1.5, 295, 423, 573, 645, 733, 903
Wavelength (Å)	1.05
Step (2θ); range (2θ) (deg)	0.05; 6–160
$(\sin\theta)/\lambda_{max}$ (Å^{-1})	0.91
Number of points	3081
Refinements	
Refinement on	$S = \sum w_i (Y_{Oi} - Y_{Ci})^2$
Weighting scheme	$w_i = 1/Y_{Oi}$
Analytical function for profile	Pseudo-Voigt
R-factors	$R_{wp} = \left\{ \frac{\sum w_i (Y_{oi} - Y_{ci})^2}{\sum w_i (Y_{oi})^2} \right\}^{\sqrt{2}}$
	$R_B = \frac{\sum \lvert I_{Ok} - I_{Ck} \rvert}{\sum I_{Ok}}$
	$GoF = [S/(N-P)]^{1/2}$
	R_{wp_c} = Modified R_{wp} taking into account the local correlations [31]
Program for refinement	XND 1.20 (see footnote 5)

were contained in a thin-walled vanadium sample can. During experiments the temperature variation was less than 1 K. The diffraction experiments were carried out at 1.5 K (M_1) in a cryostat, at room temperature (295 K, M_1) and in a furnace at 423 K (M_2), 573 K (M_3), 645 K (O_2), 733 K (T) and 903 K (C). The experiment was not performed for the O_1 phase, because of the very narrow temperature range of the existence region for this phase. Structure refinements were done using the profile Rietveld method by means of the software XND[5]. Experimental details are given in table 1.

3. Results

3.1. X-ray investigations

Evolutions of the cubic 400_c and 330_c reflections were investigated in the temperature range from 300 to 880 K. Below each ferroelastic phase transition the splitting of the lines is observed due to the appearance of ferroelastic domain structure.

Figure 2 shows the temperature evolutions of the 400_c and 330_c reflections measured from C1 and C2 samples, respectively. These reflections are single in the cubic phase. With decrease in temperature the symmetry decreases and the splitting of both types of reflection appears at transition points. It is clearly evidenced that

- the 400_c reflection
  - ∗ is single above 520 K,
  - ∗ splits into two peaks below 520 K;
- the 330_c reflection
  - ∗ is single above 850 K,

[5] A Rietveld refinement programme for real time powder diffraction patterns XND, release 1.20.

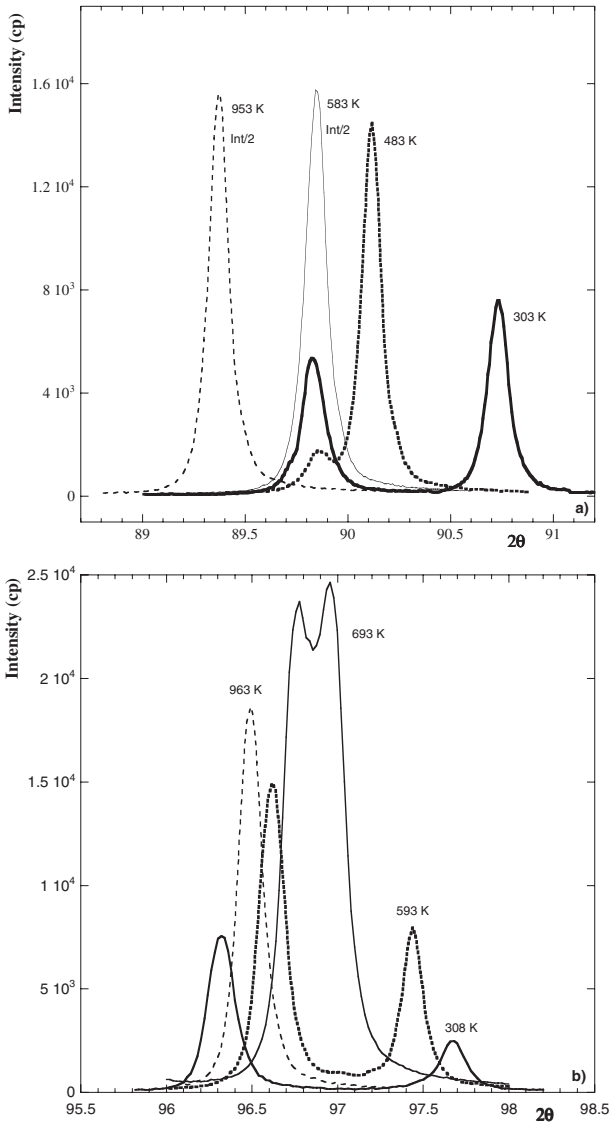

Figure 2. The temperature evolutions of 400_c (a) and 330_c (b) diffraction reflection profiles (θ–2θ scan). Int/2 indicates that the intensity is divided by two in order to fit the figure.

- ∗ divides into two not well separated peaks between 630 and 850 K,
- ∗ is observed as two well separated peaks below 630 K.

The temperature dependences of the *d*-spacings calculated from the peak angular positions of these reflections are shown in figure 3. The splitting of the 400_c reflection (figure 3(a)), which appears at 520 K, points to the M_2–M_3 phase transition. The splitting of this reflection increases with decrease of temperature. The change in the *d*-spacing variation around 630 K is related to M–O phase transition, which is associated with the rotation of the orthorhombic axes (rhombic

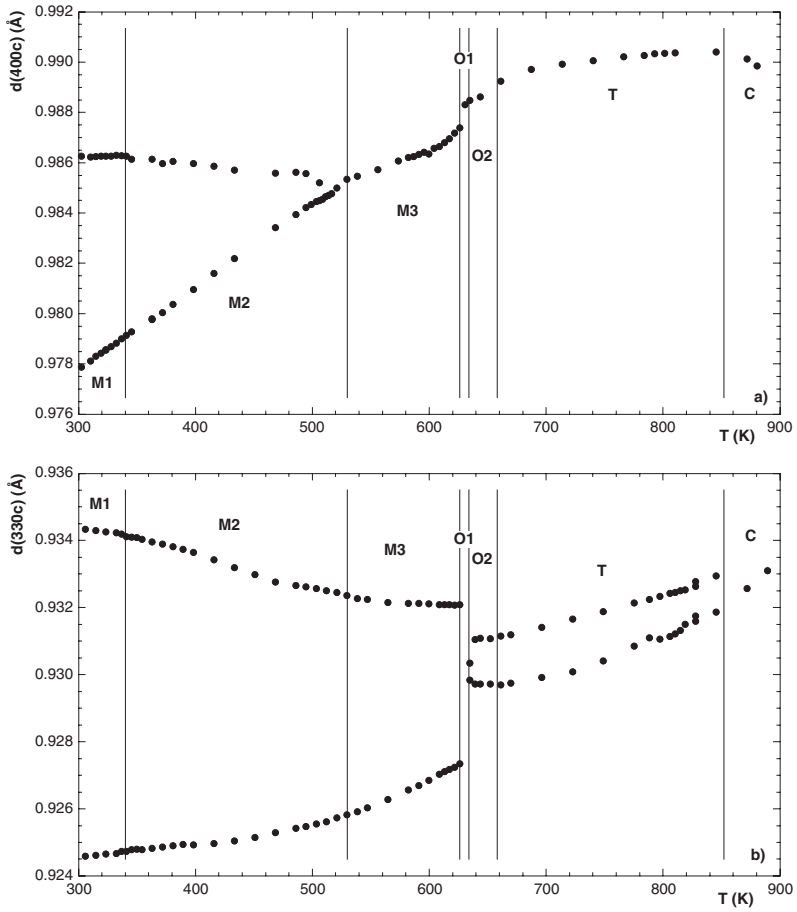

Figure 3. The temperature dependences of the d-spacings determined from peak angular positions of 400_c (a) and 330_c (b) reflections. Vertical lines indicate temperatures of the phase transitions mentioned in the introduction.

orientation $\longleftrightarrow$ parallel orientation). The existence or not of O_1 phase cannot be confirmed from these data. In addition, the splitting of the 330_c reflection around 850 K indicates the T–C phase transition. In both figures 3(a) and (b), slight anomalies are observed in the vicinity of the M_1–M_2 phase transitions. For all phases the observed reflections (θ–2θ scans) can be indexed using the unit cells reported in figure 1. The temperature evolution of the d-spacings determined from our single-crystal x-ray diffraction method is in good agreement with the pseudo-cubic cell evolution obtained from the x-ray powder diffraction technique [10, 13].

3.2. Rietveld refinements of neutron data

The diffraction patterns obtained are shown in figure 4. The diffraction lines are single in the cubic C phase. With decreasing temperature the symmetry decreases and consequently the splitting of these reflections is observed. Simultaneously, the superstructure reflections due to the multiplication of the primitive unit cell appear. It is clearly evidenced that some

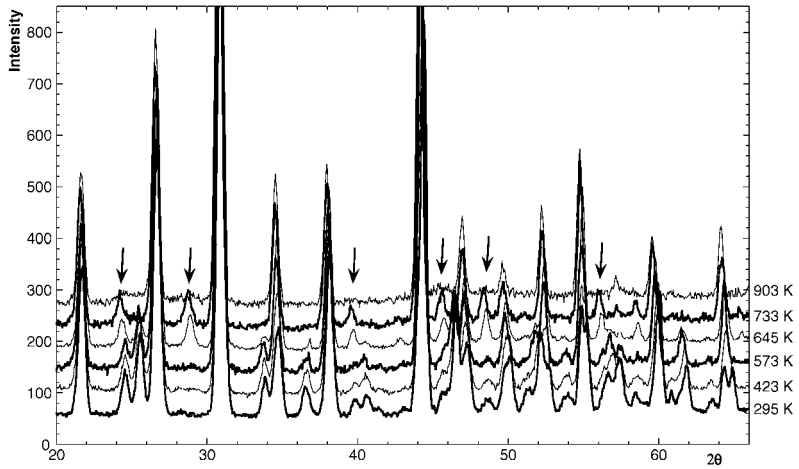

Figure 4. Neutron diffraction patterns recorded in the different phases. Arrows indicate the superstructure reflections associated with T and O phases.

superstructure reflections, characteristic for O (645 K) and T (733 K) phases, disappear at the M_3–O_1 phase transition. Instead, a new class of the superstructure reflections appears for M_1 (295 K), M_2 (423 K) and M_3 (573 K) phases (see for instance figure 4 around $2\theta \approx 54°$). It is also evidenced that the diffraction patterns recorded in M_1, M_2 and M_3 phases are very similar. In the same way, there are also slight differences between O and T phases. This is in agreement with the x-ray measurements, which show that only the M_3–O_1 and T–C transitions are well marked. For a better understanding of the phase transition sequence, we have performed Rietveld refinements for particular phases.

3.2.1. M phases. The two powder diffraction patterns recorded in the M_1 phase at 1.5 and 295 K are perfectly indexed with the $Pbcm$ space group (No 57) and the unit cell $(a_c\sqrt{2}, a_c\sqrt{2}, 4a_c)$. Starting from the atomic positions in the cubic perovskite structure, the structural refinement was led to correct R-factors (table 2, figure 5). The final structural parameters with $Pbcm$ space group are given in table 3. The refinement with the polar space group $Pbc2_1$ did not give any significant improvement. Indeed, the refinements with isotropic thermal factors for the temperature 1.5 K gave agreement R-factor values of $R_{wp} = 3.65\%$ and 3.65%, $R_{wp\_c} = 5.64\%$ and 5.61%, $R_B = 2.99\%$ and 3.00% for the $Pbc2_1$ and $Pbcm$ space groups, respectively. The correlation between the atoms, which are equivalent in the $Pbcm$ space group, was very high. The shifts from the centro-symmetric solution were of the order of the standard deviation. In a recent x-ray study [13] the monoclinic symmetry was proposed for this low temperature phase. This monoclinic symmetry has also been reported in a neutron investigation of the antiferroelectric phase (named P) of $NaNbO_3$ [17]. We have tried a possible monoclinic symmetry and refined the diffraction pattern at 1.5 K using the $P2/m$ (No 10) space group and the unit cell $(a_c\sqrt{2}, a_c\sqrt{2}, 4a_c)$. No real improvement was found ($R_{wp} = 3.61\%$, $R_{wp\_c} = 5.49\%$ and $R_B = 2.92\%$). Our neutron diffraction data, even at 1.5 K, do not allow us to distinguish between the solutions with orthorhombic and monoclinic symmetry. In our opinion, all these finding favour the space group $Pbcm$.

The diffraction patterns at 423 K (phase M_2) and 573 K (phase M_3) are very similar to each other and to that of the M_1 phase (figure 4). In the first step, the refinements were performed

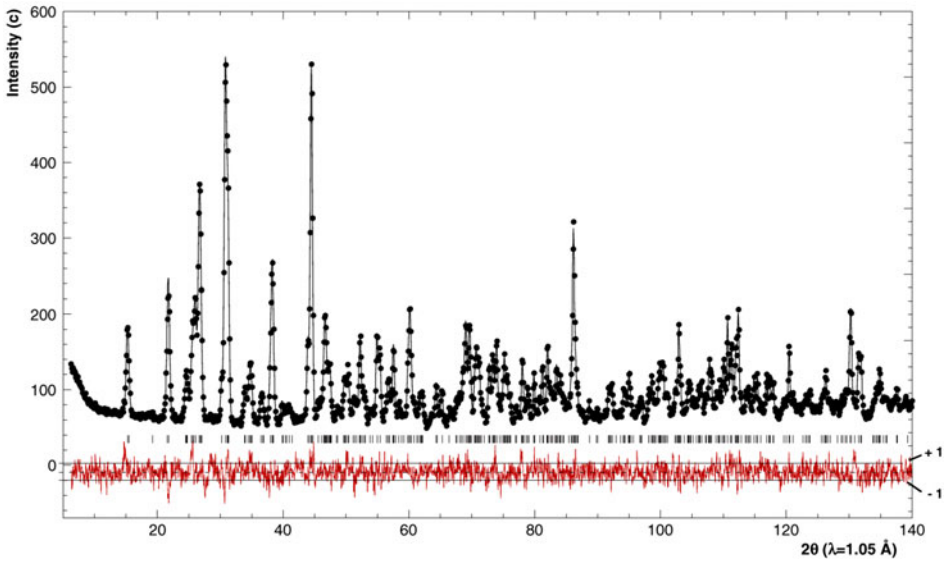

Figure 5. Rietveld refinement of neutron diffraction pattern at $T = 1.5$ K, showing the experimental (●) and the calculated profile (−). The normalized difference curve $\Delta_{norm} = (Y_{oi} - Y_{ci})/\sigma(Y_{oi})$ is plotted at the bottom. Tick lines corresponding to $\Delta_{norm} = \pm 1$ are indicated.

Table 2. *R*-factors and cell parameters obtained in the *Pbcm* space group with anisotropic thermal factors (52 structural parameters).

T (K)	R_{wp} (%)	R_{wp_c} (%)	R_B (%)	GoF	a (Å)	b (Å)	c (Å)
1.5	3.59	5.46	2.85	1.22	5.5436(3)	5.6071(3)	15.565(1)
295	3.40	4.91	2.49	1.09	5.5468(3)	5.6038(3)	15.642(1)
423	3.59	5.81	3.42	1.18	5.5498(3)	5.5979(4)	15.703(1)
573	4.43	6.20	4.23	1.08	5.5579(5)	5.5917(6)	15.771(2)

with the same space group *Pbcm* and unit cell $(a_c\sqrt{2}, a_c\sqrt{2}, 4a_c)$. Quite good agreement *R*-factors were obtained at 423 as well as at 573 K (table 2). The result for M_2 phase is fully satisfactory and confirms earlier prediction and TEM results [11].

The space groups *Pbcn* (No 60) and *Cmcm* (No 63) were proposed for the phase M_3. *Pbcn* and *Pbcm* space groups are the maximal subgroups of the *Cmcm* one. The diffraction pattern recorded at 573 K was also refined using the *Cmcm* and *Pbcn* space groups. For both cases rather poor refinement results were obtained (table 4) compared to those obtained with the *Pbcm* space group due especially to a bad fit of the majority of the weak reflections. Another possibility originating from structural studies of $NaTaO_3$ was also considered. The structure of the room temperature phase of $NaTaO_3$ is characterized by the orthorhombic symmetry in rhombic orientation, space group *Pcnm* (No 62, *Pnma*) and the cell $(a_c\sqrt{2}, a_c\sqrt{2}, 2a_c)$ [18]. These conditions gave better results than *Pbcn* or *Cmcm* but again some reflections were not well calculated. Summarizing the refinement results for the M_3 phase it may be said that the best solution was obtained for the *Pbcm* space group (table 4, figure 6). The atomic coordinates and the temperature factors obtained for this case are collected in table 3. As a conclusion of this part, one can say that the M phases are all well described with an average structure of the *Pbcm* space group.

Table 3. Structural parameters in the M phases in the *Pbcm* space group. $B_{eq} = (4/3)\sum\sum\beta_{ij}\vec{a}_i \cdot \vec{a}_j$.

Atom		1.5 K	295 K	423 K	573 K
Nb	x	0.2436(6)	0.2452(8)	0.2487(9)	0.2460(15)
	y	0.2212(3)	0.2254(3)	0.2323(4)	0.2422(10)
	z	0.1249(2)	0.1249(3)	0.1258(4)	0.1256(6)
	B_{eq} (Å^2)	0.19(2)	0.53(2)	0.86(4)	1.12(6)
Ag(1)	x	−0.2551(9)	−0.2572(12)	−0.2532(25)	−0.2507(35)
	y	1/4	1/4	1/4	1/4
	z	0	0	0	0
	B_{eq} (Å^2)	0.22(2)	1.76(3)	1.97(4)	2.78(7)
Ag(2)	x	−0.2580(10)	−0.2559(11)	−0.2561(17)	−0.2556(26)
	y	0.2211(7)	0.2311(8)	0.2359(11)	0.2428(18)
	z	1/4	1/4	1/4	1/4
	B_{eq} (Å^2)	0.47(3)	0.87(3)	1.37(4)	1.73(6)
O(1)	x	0.3109(8)	0.3065(9)	0.3086(12)	0.3022(20)
	y	1/4	1/4	1/4	1/4
	z	0	0	0	0
	B_{eq} (Å^2)	0.26(3)	0.49(3)	0.69(4)	1.31(6)
O(2)	x	−0.0348(5)	−0.0325(5)	−0.0321(7)	−0.0292(14)
	y	0.0371(5)	0.0366(5)	0.0352(7)	0.0303(14)
	z	0.1098(2)	0.1113(2)	0.1118(3)	0.1140(6)
	B_{eq} (Å^2)	0.38(3)	0.76(4)	0.97(4)	1.71(7)
O(3)	x	0.5360(5)	0.5329(5)	0.5297(7)	0.5262(13)
	y	0.4689(5)	0.4732(5)	0.4752(7)	0.4778(14)
	z	0.1396(2)	0.1389(2)	0.1379(3)	0.1375(5)
	B_{eq} (Å^2)	0.35(3)	0.56(3)	0.93(4)	1.17(6)
O(4)	x	0.1944(8)	0.1991(10)	0.2072(14)	0.2155(23)
	y	0.2678(7)	0.2692(8)	0.2676(12)	0.2622(24)
	z	1/4	1/4	1/4	1/4
	B_{eq} (Å^2)	0.39(3)	0.96(3)	1.31(4)	1.67(7)

Table 4. R-factors obtained at 573 K (phase M_3) for the proposed space groups (anisotropic thermal factors).

Space group	R_{wp} (%)	R_{wp_c} (%)	R_B (%)	GoF	Number of struc. par.
Cmcm	9.85	28.9	16.6	2.39	34
Pbcn	6.66	16.0	12.0	1.62	52
Pcnm[a]	5.74	11.7	8.1	1.40	30

[a] Cell ($a_c\sqrt{2}, a_c\sqrt{2}, 2a_c$).

3.2.2. O phases. As was pointed out in experimental procedures the diffraction experiment was carried out only for the O_2 phase (645 K). This phase is orthorhombic in parallel orientation with axes along the [100] pseudo-cubic direction. The diffraction pattern can be indexed with the unit cell ($2a_c, 2a_c, 2a_c$). For such diffraction conditions the expected space groups are *Pmnm* (No 59, *Pmmn*) and *Cmcm* (No 63). These two space groups do not have the same reflection conditions; nevertheless, the differences between the cell parameters are too weak to make a choice without ambiguity. Therefore, these two possibilities were considered. When thermal factors were taken as isotropic, the better solution was obtained for the primitive space

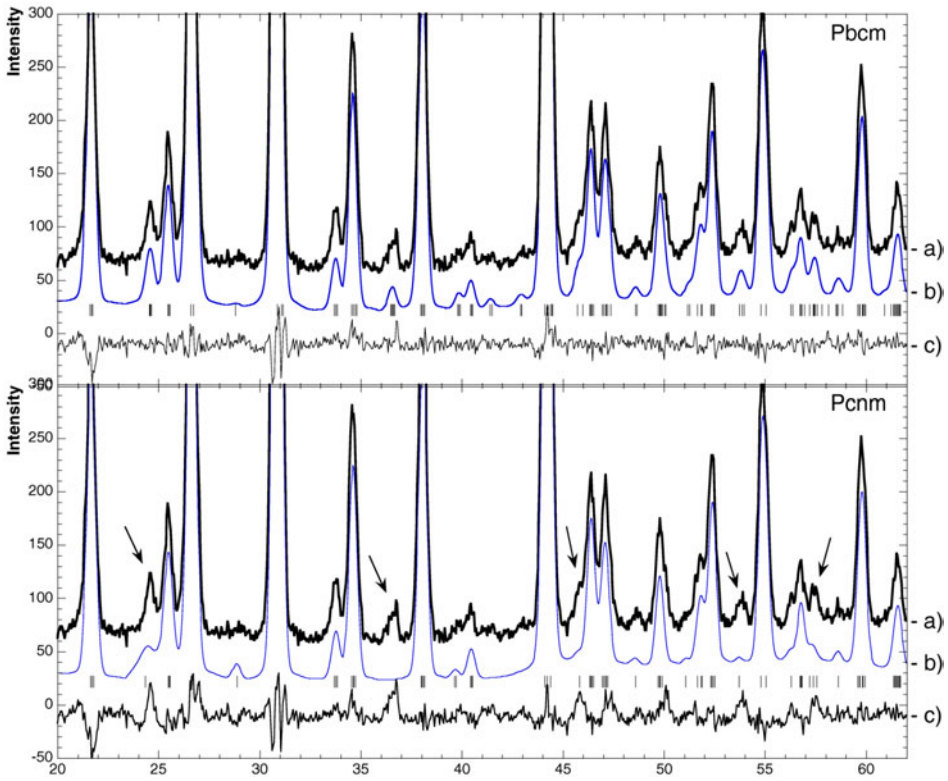

Figure 6. Comparison between the *Pcnm* and *Pbcm* solutions for the M_3 phase. Experimental (a), calculated (b) and difference (c) profiles. Arrows show some not well refined reflections with *Pcnm* space group.

Table 5. *R*-factors obtained at 645 K (phase O_2) with isotropic (i) or anisotropic (a) thermal motion.

Space group	R_{wp} (%)	R_{wp_c} (%)	R_B (%)	GoF	Number of struc. par.
Cmcm (i)	4.27	11.37	8.33	1.96	16
Pmnm (i)	3.33	7.11	5.52	1.53	29
Cmcm (a)	3.00	5.54	3.68	1.38	34
Pmnm (a)	2.91	5.14	3.28	1.35	64

group *Pmnm* than for the centred *Cmcm* one (table 5). Nevertheless, in the case of the *Cmcm* space group, an introduction of anisotropic thermal factors leads to a correct result (table 5) with an equivalent number of parameters to be refined (29 for *Pmnm* isotropic compared to 34 for *Cmcm* anisotropic). In the case of *Pmnm* the introduction of anisotropic thermal factors is not easy because the correlations between parameters are high and some ellipsoids are not positively defined. Therefore, the choice of *Cmcm* space group seems to be more correct. The structural parameters corresponding to this space group are given in table 6.

Table 6. Structural and cell parameters at 645 K ($Cmcm$), 733 K ($P4/mbm$) and 903 K ($Pm\bar{3}m$). $B_{eq} = (4/3)\sum\sum\beta_{ij}\vec{a}_i \cdot \vec{a}_j$.

Atom		645 K	733 K	903 K
Nb	x	1/4	0	0
	y	1/4	0	0
	z	0	0	0
	B_{eq} (Å^2)	1.31(4)	1.38(4)	1.63(2)
Ag(1)	x	0	0	1/2
	y	−0.001(2)	1/2	1/2
	z	1/4	1/2	1/2
	B_{eq} (Å^2)	1.98(6)	2.80(3)	3.47(4)
Ag(2)	x	0		
	y	0.494(3)		
	z	1/4		
	B_{eq} (Å^2)	3.54(8)		
O(1)	x	0.2827(7)	0	0
	y	1/4	0	0
	z	0	1/2	1/2
	B_{eq} (Å^2)	2.27(5)	3.14(5)	3.60(4)
O(2)	x	0	0.2782(3)	
	y	0.2259(8)	0.2218(3)	
	z	0.0205(8)	0.0358(4)	
	B_{eq} (Å^2)	1.94(4)	2.08(4)	
O(3)	x	0.2710(7)		
	y	0.2456(11)		
	z	1/4		
	B_{eq} (Å^2)	2.56(6)		
Cell	a (Å)	7.883(1)	5.5815(3)	3.9598(3)
	b (Å)	7.890(1)		
	c (Å)	7.906(1)	3.9595(3)	

3.2.3. T phase. The refinements based on the unit cell ($a\sqrt{2}, a\sqrt{2}, c$) and the space group $P4/mbm$ (No 127) led to rather high R-factor values ($R_{wp} = 6.6\%$, $R_{wp\_c} = 15.6\%$, $R_B = 13.5\%$). In a recent paper [13] the space group $I4/mcm$ (No 140) with the unit cell parameters ($a\sqrt{2}, a\sqrt{2}, 2c$) was proposed. However, this space group should be excluded because the indexation rule (hkl: $h + k + l = 2n$) is not verified (figure 7). Moreover, as the diffraction pattern gave no evidence of any reflections with $l = 2n + 1$ corresponding to the doubling of the c-axis, we have also excluded the primitive tetragonal subgroups of $I4/mcm$ ($a\sqrt{2}, a\sqrt{2}, 2c$), the tetragonal subgroups with c doubled of $P4/mbm$($a\sqrt{2}, a\sqrt{2}, c$) and the $Cmcm$ ($2a$, $2b$, $2c$) space group of the orthorhombic symmetry as no splitting of reflections was observed.

Finally, we have carried on with the $P4/mbm$ space group by introducing anisotropic thermal factors (tables 6 and 7). An important improvement was achieved as the R-factors strongly decrease from $R_{wp} = 6.6\%$, $R_{wp\_c} = 15.6\%$, $R_B = 13.5\%$ to $R_{wp} = 4.8\%$, $R_{wp\_c} = 7.1\%$, $R_B = 6.25\%$. The biggest anisotropic thermal factors were obtained for the oxygen ions (figure 8). The thermal ellipsoids obtained were large, which indicates that the ordered $P4/mbm$ phase is not sufficient to describe the T phase. We have then tested the possibility of a coexistence of both $P4/mbm$ and $I4/mcm$ phases. After refinement, the

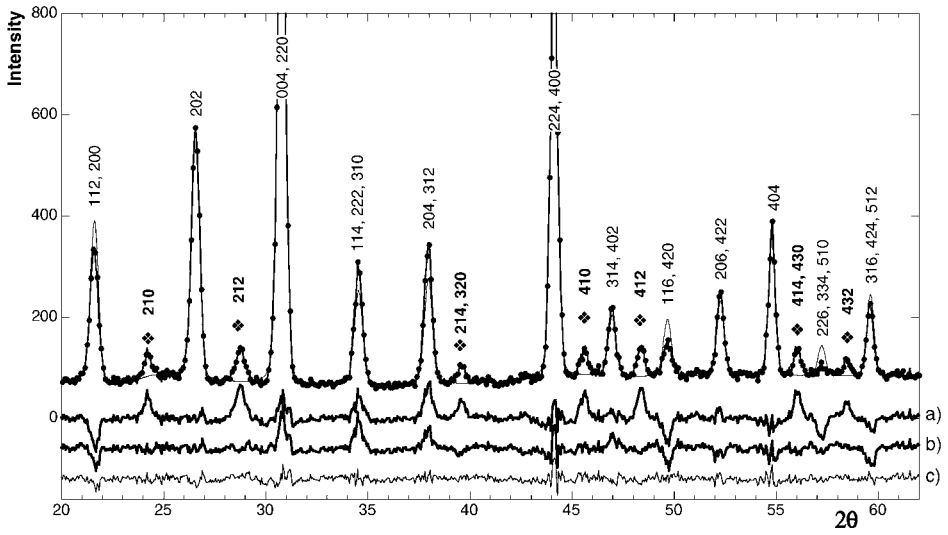

Figure 7. Diffraction pattern of the T phase showing the occurrence of $h+k+l=2n+1$ (marked in the figure) in disagreement with the I centring. The normalized difference curves are plotted for $I4/mcm$ (a), $P4/mbm$ (b) and $P4/mbm$ with anharmonic terms (c) space groups.

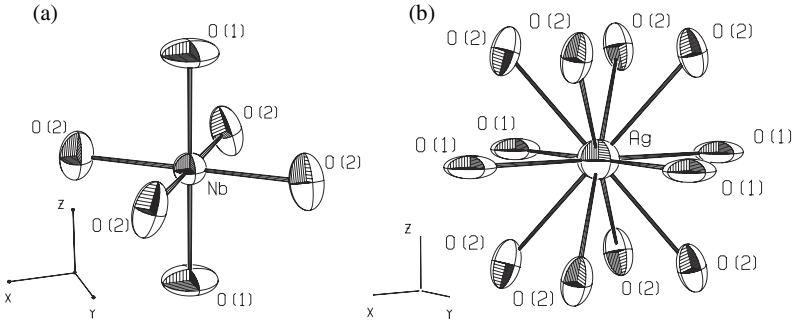

Figure 8. Drawing of anisotropic thermal ellipsoid in T phase ($P4/mbm$ space group). Nb (a) and Ag (b) environment.

Table 7. R-factors at 733 K (phase T) and 903 K (phase C). anh: anharmonic thermal factors.

T (K)	Space group	R_{wp} (%)	R_{wp_c} (%)	R_B (%)	GoF	Number of struc. par.
903	$Pm\bar{3}m$ (a)	5.00	7.07	3.90	1.09	5
903	$Pm\bar{3}m$ (anh)	4.92	6.69	3.13	1.07	13
733	$P4/mbm$ (a)	4.77	7.11	6.25	1.15	12
733	$P4/mbm$ (anh)	4.59	6.23	4.87	1.11	27

contribution obtained for the $I4/mcm$ phase was very weak (5%) and the improvement was not significant compared to the sole phase $P4/mbm$ solution ($R_{wp}=4.70\%$ instead of 4.77%). The large thermal ellipsoids can then be an indication of atomic disorder.

In the electron microscopy study, Verwerft *et al* [11] have observed diffuse scattering above the orthorhombic–tetragonal phase transition. They have assumed that the oxygen octahedron tilts around the *c*-axis are correlated within each layer perpendicular to the *c*-axis but they are not correlated from one layer to another along the *c*-axis. The rather high value of R_B-factor (6.25%) for the T phase (in agreement with the observation of large thermal ellipsoids on figure 8), in comparison to those of other phases, suggests the possibility of an existence of atomic disorder. Indeed, for instance (table 7) the R_{wp}-factors of the anisotropic structure of both the cubic and tetragonal phases are rather comparable whereas the R_B-factors are quite obviously different.

The atomic disorder can be taken into account either by considering atoms in multi-well potentials around their Wyckoff positions or by introducing anharmonic terms of thermal motion. We have preferred the second more general approach. We have used the Gram–Charlier expansions method by introducing in the thermal factor the third order or the fourth order if the third order is null due to the symmetry conditions. A significant decrease of R_B-factor and an improvement of R_{wp} were obtained (table 7). The intensity of the reflections is better calculated as one can see in figure 7. The anharmonic thermal parameters of Ag and Nb are very weak compared to the ones of the oxygen and confirm a positional disorder of these atoms in the tetragonal phase.

3.2.4. C phase. A correct refinement of the diffraction pattern recorded in the cubic C phase (at 903 K) was obtained. The space group $Pm\bar{3}m$ (No 221) and a primitive perovskite unit cell were considered. The results of the refinements are presented in tables 6 and 7. The introduction of anharmonic terms leads to a small improvement. The refinements have not pointed to any disorder in this phase.

4. Discussion and conclusion

Our x-ray and neutron diffraction investigations of silver niobate $AgNbO_3$ confirmed the existence of a sequence of phase transitions. As in previous structural studies [10, 11], the experiments performed pointed to M_3–O_1, O_2–T and T–C phase transitions related to essential structural changes and did not give significant proofs for the M_1–M_2 phase transition. The M_2–M_3 phase transition was only observed in the 400_c evolution (figure 3). The Rietveld refinements of the neutron diffraction patterns allowed us to determine for the first time the crystal structure of particular phases of $AgNbO_3$. In the first part of the discussion the high temperature phase transitions are described. In the second part we will try to explain the problem of 'unobservable' transitions between the M phases.

Geometrical considerations [26, 27] pointed that in $AgNbO_3$, similarly as in $NaNbO_3$, the main mechanism of *displacive* structural phase transitions should be connected with tilts of the nearly rigid oxygen octahedra. Such a case is experimentally found. Starting from the high temperature cubic phase, the tetragonal symmetry appears as a result of the oxygen octahedron tilts around the *c* axis (figure 9). Using the Glazer notation [28], the scheme of the octahedron tilts in the tetragonal T phase is $a^0a^0c^+$. However, taking into account the problems with refinements, the use of anharmonic thermal factors was necessary. This may be interpreted as the appearance of structural disorder. Earlier, Werwerft and co-workers proposed to connect diffuse scattering observed in $AgNbO_3$ with disorder in the oxygen sublattice [11]. Our results are in agreement with this since they show that the positional disorder concerns principally the oxygen atoms. The disorder in the T phase can be related to frequent appearance of local anti-phase tilts ($a^0a^0c^-$) where an additional disordered oxygen octahedron appears. Here,

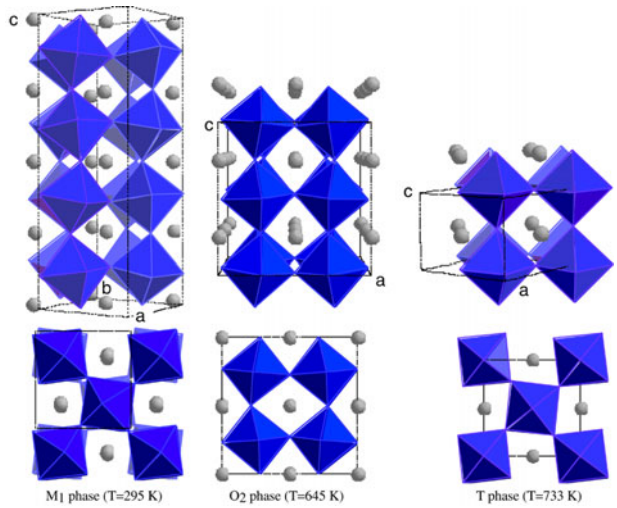

Figure 9. Schematic drawing of the oxygen octahedron tilts in T, O_2 and M_1 phases. The Nb and Ag ions are omitted.

an important question must be stated. Is disorder present in the tetragonal phase only, or is it frozen and influencing the structure and properties of the lower phases? The existence of discommensurations at room temperature detected in TEM investigations [29] and the spectroscopic studies [5, 7] support the latter possibility. On the other hand, our refinements point to the presence of atomic disorder only for the T phase and perhaps for the O_2 phase. The introduction of anisotropic thermal factors gives essential improvement only for these phases. At 1.5 K, the thermal factors are small and quite normal. This apparent contradiction can be explained if we consider that these different techniques do not give access to the same information. The discommensurations do not give observable phenomena in powder diffraction refinements. The dielectric properties are very sensitive to local polar order. If small ion displacements are correlated only in the nanoscale then local polar order can give a significant effect in spectroscopic dielectric studies. On the other hand, the appearing disorder cannot give marked effects in diffraction studies. This is the situation of relaxor compounds such as $BaTi_{0.65}Zr_{0.35}O_3$ where the atomic displacements responsible for the appearance of the local polar order are too small to induce big thermal factors [30]. The disorder in T and O_2 phases is principally related to the local faults of the oxygen octahedron tilt scheme. This disorder lessens to the transition T $\rightarrow$ O with the condensation of octahedron tilts in the *b*-direction, and it disappears in the M phases. In the M phases there only remains a small positional atomic disorder with a local polar behaviour, which certainly implicates Nb and Ag atoms.

Further decrease in temperature causes the appearance of the additional oxygen octahedron tilts around draw *b*-axis at the O_2–T phase transition. In the orthorhombic O_2 phase the Nb ions stay in the octahedron centres while the Ag ions are slightly displaced along the *b*-axis (table 6). The scheme of the octahedron tilts is described as $a^0b^-c^+$ and shown in figure 9. For reasons given earlier the orthorhombic O_1 phase is not under investigation.

The most significant structural changes take place at the M_3–O_1 phase transition. The orthorhombic M_3 phase appears mainly as further oxygen tilts along the *a* cubic axis. The oxygen tilting system corresponds to successive $(a^-b^-c^+)/(a^-b^-c^-)$ (belonging to the same

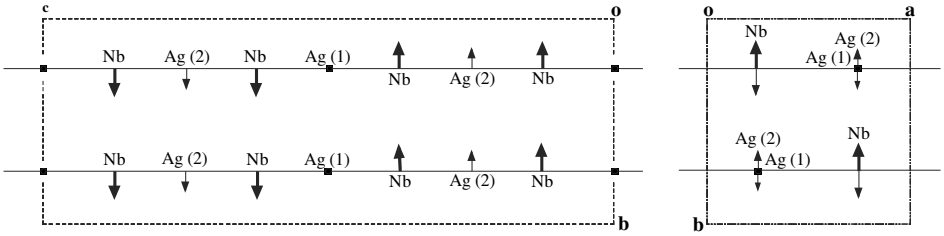

Figure 10. Schematic drawing of the antiparallel Nb and Ag ion displacements in M_1 phase.

unit cell) rotations along the *c*-direction. In addition, the Ag and Nb ions shift in the $[110]_c$ cubic direction (direction near the *b*-axis). Due to the antiparallel Nb and Ag ion displacements an antiferroelectric state appears (figure 10).

In general, the symmetry, multiplication of formula unit cell and crystal structure of $AgNbO_3$ in all M phases are very close to each other and very similar to that of antiferroelectric (phase P) $NaNbO_3$. No significant difference is found in the refinement between the M phases. The same long range average structure has been obtained in the three phases. Only the amplitude of atomic displacement increases appreciably from M_3 phase to M_1 phase. These phases do not show important atomic oxygen disorder like the high temperature phases. The change observed in the 400_c evolution is due to the increasing of the orthorhombic distortion at the M_3–M_2 transition. The ferroelectric behaviour attributed to the M_3 phase is either too small to induce an observable effect in the refinements or more probably has a local character without long range order, in agreement with spectroscopy studies.

As a conclusion, our structural investigation has evidenced the average phases in the well known $AgNbO_3$ compound. This study has also shown a strong structural disorder dominated by the oxygen octahedra in the paraelectric T and O phases and by the cations Ag and Nb in the low temperature non-paraelectric M phases. Displacements of Ag and especially Nb are considered to be responsible for the polar and/or anti-polar character of the low temperature M phases. Indeed, no oxygen disorder has been evidenced in the M phases in which all oxygen tiltings have condensed in the long range. The paraelectric phase (T, O_2, O_1) sequence in $AgNbO_3$ can then be interpreted as a successive condensation of oxygen octahedral tilts. In the M phases antiparallel cationic displacements are connected to the long range antiferroelectric state. Nevertheless, due to some defects, Ag vacancies for instance, a local polar order can exist in a cluster form. The relaxor behaviour observed is then a consequence of polar clusters embedded into an antiferroelectric phase. Of course, the above scenario remains speculative and further experimental investigations are clearly needed to understand in more detail the mechanisms leading to local structural deviations within the average structure.

References

[1] Valant M and Suvorov D 1998 *J. Am. Ceram. Soc.* **82** 88
[2] Petzelt J, Kamba S, Buixaderas E, Bovtun V, Zikmund Z, Kania A, Koukal V, Pokorny J, Polivka J, Pashkov V, Komandin G and Volkov A 1999 *Ferroelectrics* **223** 235
[3] Valant M, Suvorov D, Hoffmann C and Sommariva H 2001 *J. Eur. Ceram. Soc.* **21** 2647
[4] Kim H T, Shrout T, Randall C and Lanagan M 2002 *J. Am. Ceram. Soc.* **85** 2738
[5] Volkov A A, Gorshunov B P, Komandin G, Fortin W, Kugel G E, Kania A and Grigas J 1995 *J. Phys.: Condens. Matter* **7** 785
[6] Kania A 2001 *J. Phys. D: Appl. Phys.* **34** 1447
[7] Hafid M, Kugel G E, Kania A, Roleder K and Fontana M D 1992 *J. Phys.: Condens. Matter* **4** 2333

[8] Kania A 1983 *Phase Transit.* **3** 131
[9] Francombe M H and Lewis G 1958 *Acta Crystallogr.* **11** 175
[10] Pawelczyk M 1987 *Phase Transit.* **8** 273
[11] Verwerft M, Van Dyck D, Brabers V A M, Van Landuyt J and Amelinckx S 1989 *Phys. Status Solidi* a **112** 451
[12] Kania A 1998 *Ferroelectrics* **205** 19
[13] Ratuszna A, Pawluk J and Kania A 2003 *Phase Transit.* **76** 611
[14] Glazer A M and Megaw H D 1973 *Acta Crystallogr.* A **29** 489
[15] Megaw H D 1974 *Ferroelectrics* **7** 87
[16] Glazer A M and Ishida K 1974 *Ferroelectrics* **6** 219
[17] Darlington C N W and Knight K S 1999 *Physica* B **226** 368
[18] Darlington C N W and Knight K S 1999 *Acta Crystallogr.* B **55** 24
[19] Miga S and Dec J 1999 *J. Appl. Phys.* **85** 1756
[20] Fabry J, Zikmund Z, Kania A and Petricek V 2000 *Acta Crystallogr.* C **56** 916
[21] Sakowski-Cowley A C, Lukaszewicz K and Megaw H D 1969 *Acta Crystallogr.* B **25** 851
[22] Darlington C N W 1999 *Powder Diffr.* **14** 253
[23] Petzelt J, Kamba S and Gregora I 1997 *Phase Transit.* **63** 107
[24] Tagantsev A K 1988 *Ferroelectrics* **79** 57
[25] Kania A 1989 *J. Cryst. Growth* **96** 703
[26] Kassan-Ogly F A and Naish V E 1986 *Acta Crystallogr.* B **42** 307
[27] Thomas N W 1989 *Acta Crystallogr.* B **45** 337
[28] Glazer A M 1972 *Acta Crystallogr.* B **28** 3384
[29] Verwerft M, Van Tendeloo G, Van Landuyt J, Coene W and Amelinckx S 1988 *Phys. Status Solidi* a **109** 67
[30] Sciau Ph and Castagnos A M 2002 *Ferroelectrics* **270** 259
[31] Bérar J F and Lelann P 1991 *J. Appl. Crystallogr.* **24** 1